https://doi.org/10.5194/wes-2024-56
Preprint. Discussion started: 15 May 2024

Open Access
WIND ENERGY SCIENCE
DISCUSSIONS

On the robustness of a blade load-based wind speed estimator to dynamic pitch control strategies

Marion Coquelet[1,2,3], Maxime Lejeune[1], Laurent Bricteux[2], Aemilius van Vondelen[3], Jan-Willem van Wingerden[3], and Philippe Chatelain[1]

[1]Institute of Mechanics, Materials and Civil Engineering, UCLouvain, Louvain-la-Neuve, Belgium
[2]Fluids-Machines Department, UMONS, Mons, Belgium
[3]Delft Center for Systems and Control, TU Delft, Netherlands

Correspondence: Marion Coquelet (m.coquelet@tudelft.nl)

Abstract. Current implementations of wind turbine pitch controllers for load alleviation or active wake mixing use limited information about the incoming wind. While these pitch controllers could benefit from broader wind condition awareness, the lack of suitable sensing methods is limiting. Blade load-based wind speed estimators are an alternative to cup anemometers or LiDARs. In this paper, we wish to verify how robust such estimators are to the control strategy active on the turbine, as it impacts both operating parameters and loads. We use an Extended Kalman Filter (EKF) to estimate incoming wind conditions based on blade out-of-plane bending moments. The internal model in the EKF relies on the Blade Element Momentum (BEM) theory in which we propose to account for delays between pitch action and blade loads by including dynamic effects. Using Large-Eddy Simulations to test the estimator, we show that accounting for the dynamic effects in the BEM formulation is needed to maintain the estimator accuracy when dynamic wake mixing control is active.

1 Introduction

With their 2030 Agenda for Sustainable Development, the United Nations (2015) set 17 Goals to ensure Sustainable Development of our planet. Sustainable Development Goal number 7 aims at ensuring access to affordable, reliable, sustainable and modern energy for all. In that perspective, reducing the Levelized Cost of Energy (LCoE) coming from wind is essential. Two factors contributing to this effort are considered here: increasing wind power capture at farm scale and reducing the occurrence of failures on turbines. Wind turbine and wind farm flow control can contribute to these two objectives.

Individual Pitch Control (IPC) has shown its potential to reduce structural loads, from numerical studies (Bossanyi, 2003) to experimental demonstrations (Bossanyi et al., 2013). In the mean time, several wind farm flow control strategies have been considered to mitigate wake effects and maximize power production in wind farms. Static flow control was originally proposed, mostly wake redirection using yaw control (Fleming et al., 2014; Wagenaar et al., 2012). Dynamic flow control has also been investigated, mostly the Pulse approach and the Helix approach. The first one, the Pulse, relies on collective pitch control to periodically vary the thrust force of the turbine, at a frequency that is typically one order of magnitude smaller than the turbine rotation frequency (Yilmaz and Meyers, 2018; Munters and Meyers, 2018). The resulting changes in induction generate pulsating patterns in the wake, which help it destabilize faster. When it comes to the Helix approach, individual pitch control is

https://doi.org/10.5194/wes-2024-56
Preprint. Discussion started: 15 May 2024

used to generate sinusoidal variations of the tilt and yaw moments in quadrature phase (Frederik et al., 2020). It follows from this actuation that the wake is displaced laterally as it propagates downstream, taking the shape of a helix, and that its recovery is also enhanced (Korb et al., 2023). Both strategies come with additional loading and pitch bearing activity (Frederik and van Wingerden, 2022; van Vondelen et al., 2023b).

Let us focus the remainder of this review on pitch actuation-based control strategies, for which wind conditions awareness is often very limited. In the case of load alleviation using IPC, some studies proposed controllers including explicit information about the incoming wind, such as the rotor-effective wind speed measured by a LiDAR in Russell et al. (2024). Still, for most IPC controllers, the measurements used to determine the control actions are the blade loads (Bossanyi, 2003; Lu et al., 2015). When it comes to dynamic wake mitigation, the Pulse and the Helix strategies act in an open-loop manner, imposing kinematic laws on pitch actuation. Information on the flow conditions, whether explicitly or through blade loads, is not used.

Yet wind conditions awareness could be essential to develop more efficient controllers (Meyers et al., 2022). When it comes to load alleviation, Selvam et al. (2009) showed that including a feedforward loop based on wind disturbance estimation in the IPC scheme benefited the reduction of structural loads. Russell et al. (2024) additionally demonstrated how LiDAR-assisted feedforward individual pitch control was improving load alleviation results for turbines operating in freestream conditions. Coquelet et al. (2022) investigated the case of waked turbines and concluded that it provided challenges, calling for new IPC schemes accounting for partial or total wake impingement. When it comes to wake mixing, the controllers act in a dynamic way. How the actuation is phased with respect to turbulent structures in the incoming flow therefore influences their efficiency in alleviating wake effects. Munters and Meyers (2018) for instance showed, using an optimal control framework for dynamic induction control, that the vortex rings generated by the optimal controller coincide with bulges that are naturally present in the wake of the reference case. The turbine actuation thus phases itself with the incoming turbulent flow structures. van Vondelen et al. (2023a) and Korb et al. (2023) also showed, in the context of a line of three turbines, that the pitch phase offset between the first and the second turbine influences the power leveraged for the third turbine. The capability to sense the incoming flow would thus represent a step towards smarter implementation of such controllers, in turn opening the door to more efficient energy harvesting.

Though these examples highlight the potential of wind conditions awareness in the context of wind turbine and wind farm flow control, they still lack practical implementation. It appears that today's turbines are still little informed about the wind flow impinging them. In practice, nacelles are generally equipped with simple measurement devices such as anemometers (Bottasso et al., 2018). These provide information on the wind at the measurement point, making turbines unaware of wake impingement, shear or turbulent gusts. Their measurements additionally suffer from a number of disturbances ranging from the presence of the nacelle or blades to the wake-induced flow deformations resulting in unreliable measurements. Nacelle-mounted LiDARs have consequently been receiving growing attention as they propose an interesting alternative to these simple measurement devices. They offer remote sensing and are able to provide a great characterization of the future incoming flow, enabling feedforward approaches (Letizia et al., 2023; Scholbrock et al., 2016). Though industrial use of LiDARs for control applications has been reported (Raach, 2021), their cost, complexity of installation, or need for synchronization with the SCADA system still limit their broad use.

https://doi.org/10.5194/wes-2024-56
Preprint. Discussion started: 15 May 2024

Alternative methods, relying on sensors readily available on modern wind turbines, are thus worth investigating. This idea is at the base of the rotor-as-a-sensor approach, which relies on the principle that any change in the wind is reflected on the load response of the rotor. At a more local scale, blades can be seen as rotating sensors whose bending moments are used to estimate the local inflow wind speed, further referred to as the blade-effective wind speed. Several contributions on the topic rely on estimators deriving from Kalman filters. Simley and Pao (2016) present a linear Kalman filter-based estimator for estimation of hub-height wind speed and wind shear components. Interestingly, the authors show that the estimator performances degrade when blade pitch actuation occurs due to the nonlinearities appearing in the turbine response. Bottasso et al. (2018) introduce an extended Kalman filter (EKF) formulation to estimate blade-effective wind speeds. These are then transformed into sector-effective wind speeds for wake detection application. In Bertelè et al. (2017), this approach is extended to the estimation of inflow misalignment and shear angles through the identification of the blade load harmonics. The EKF approach is also reported in Lejeune et al. (2022), where the sensing is used to infer flow information to a meandering-capturing wake model developed for operational wind farm flow prediction. In Brandetti et al. (2023), it is an unscented Kalman filter that is used for blade-effective wind speed estimation on vertical-axis wind turbines. Other types of estimators have also been reported, such as a subspace predictive repetitive estimator in Liu et al. (2021) and both a proportional integral notch estimator and a Coleman-based estimator in Liu et al. (2022).

This work investigates the ability of these blade load-based estimators to infer the characteristics of the incoming wind when the turbine is operated with different advanced control strategies. Indeed, the underlying principle of load-alleviation IPC, the Pulse and the Helix is to use pitch actuation to modify blade loads. We wonder whether a blade load-based estimator can still be accurate in that context and therefore be used for closed-loop control applications. To answer this question, we deploy an EKF using the blade out-of-plane bending moments to estimate wind speed both at the rotor scale and at more local scales, building up on the work of (Bottasso et al., 2018). Kalman-filter based estimators rely on an internal model of the turbine relating the measurements and the estimations. Linearized models cover only a small range of turbine operation and lead to inaccuracies out of that range (Simley and Pao, 2016; van Vondelen et al., 2023a), while nonlinear look-up tables Bottasso et al. (2018); Liu et al. (2021) cannot account for dynamic effects between actuation and loads. Regarding the dynamic pitching context is which this paper falls, we propose the use of a dynamic BEM formulation, covering the whole range of operation of the turbine and accounting for potential delays between pitch actuation and blade loads. We demonstrate the performance of the estimator using Large-Eddy Simulation (LES). The simulated blade bending moments and turbine operating parameters are fed to the estimator and the wind speed estimates are validated against the actual velocity field retrieved from the LES. We then verify the accuracy of the estimator in cases where pitch control strategies are active for load alleviation and for wake mixing.

The contributions are thus threefold:

1. Formulate a blade load-based estimator using a BEM as the internal model in the EKF.

https://doi.org/10.5194/wes-2024-56
Preprint. Discussion started: 15 May 2024

2. Include dynamics in the BEM to account for delays between pitch action and blade loads in the context of dynamic pitch control.

3. Verify the robustness of this estimator to load alleviation and wake mixing control strategies in LES.

The remainder of the paper is organized as follows. Section 2 introduces the EKF and the testing environment. The performances of the estimator on a single turbine immersed in turbulent wind are assessed in Sec. 3. The robustness of the blade load-based estimator is evaluated for turbines using load alleviation and wake mixing control in Sec. 4. Eventually, conclusions are drawn alongside perspectives in Sec. 5.

2 Methodology

This section presents the structure of the blade load-based estimator and briefly describes the LES environment in which it is tested.

2.1 Extended Kalman Filter for wind speed estimation

The general procedure of the EKF theory is recalled before being applied to the estimation of blade-effective wind speeds. How the latter are then used to reconstruct several characteristics of the wind speed impinging on the rotor is eventually presented.

2.1.1 Extended Kalman Filter

Consider the discrete-time state-space representation of a nonlinear system

$$\boldsymbol{x}_k = \boldsymbol{f}\left(\boldsymbol{x}_{k-1}, \boldsymbol{u}_{k-1}\right) + \boldsymbol{w}_{k-1}, \tag{1}$$

$$\boldsymbol{y}_k = \boldsymbol{h}\left(\boldsymbol{x}_k, \boldsymbol{u}_k\right) + \boldsymbol{v}_k, \tag{2}$$

with $\boldsymbol{x}_k$ the state vector at time instant k, $\boldsymbol{y}_k$ the output or measurement vector, $\boldsymbol{u}_k$ the control input vector. $\boldsymbol{f}\left(\boldsymbol{x}_{k-1}, \boldsymbol{u}_{k-1}\right)$ is the nonlinear state function and $\boldsymbol{h}\left(\boldsymbol{x}_k, \boldsymbol{u}_k\right)$ is the measurement function. $\boldsymbol{w_k}$ is the process noise vector and $\boldsymbol{v_k}$ is the measurement noise vector. In EKF theory, they are assumed to be zero-mean Gaussian white noise with covariance matrices $\boldsymbol{Q}$ and $\boldsymbol{R}$, respectively (Chui et al., 2017).

The purpose of the EKF is to compute an estimate of the unknown states $\boldsymbol{x}$ based on the system model and input/output signals. It is an extension of the linear Kalman filter in the sense that it generalizes the formulation to nonlinear systems. To do so, it relies on the Jacobian matrices of the state and measurement functions, for the prediction and correction step respectively (Chui et al., 2017).

The prediction step at time k consists in computing the *a priori* error covariance estimate $\boldsymbol{P}_k^-$ and the *a priori* state estimate $\hat{\boldsymbol{x}}_k^-$, based on the previous estimates of the covariance matrix $\boldsymbol{P}_{k-1}^+$ and the state $\hat{\boldsymbol{x}}_{k-1}^+$, and the Jacobian matrix of the state

https://doi.org/10.5194/wes-2024-56
Preprint. Discussion started: 15 May 2024

WIND ENERGY SCIENCE DISCUSSIONS

function $\boldsymbol{F}_{k-1}$. The computation is as follows:

$$\boldsymbol{F}_{k-1} = \left.\frac{\partial \boldsymbol{f}}{\partial \boldsymbol{x}}\right|_{\hat{\boldsymbol{x}}^+_{k-1},\boldsymbol{u}_{k-1}} \tag{3}$$

$$\boldsymbol{P}^-_k = \boldsymbol{F}_{k-1}\boldsymbol{P}^+_{k-1}\boldsymbol{F}^T_{k-1} + \boldsymbol{Q} \tag{4}$$

$$\hat{\boldsymbol{x}}^-_k = \boldsymbol{f}\left(\hat{\boldsymbol{x}}^+_{k-1},\boldsymbol{u}_{k-1}\right) \; . \tag{5}$$

The correction step then makes use of the measurement $\boldsymbol{z}_k$ to compute the *a posteriori* state estimate $\hat{\boldsymbol{x}}^+_k$ and the *a posteriori* error covariance matrix $\boldsymbol{P}^+_k$, based on the Jacobian matrix of the measurement function $\boldsymbol{H}_k$, the measurement residual $\tilde{\boldsymbol{y}}_k$ and the Kalman gain $\boldsymbol{K}_k$. The procedure is as follows:

$$\boldsymbol{H}_k = \left.\frac{\partial \boldsymbol{h}}{\partial \boldsymbol{x}}\right|_{\hat{\boldsymbol{x}}^-_k,\boldsymbol{u}_k} \tag{6}$$

$$\boldsymbol{K}_k = \boldsymbol{P}^-_k\boldsymbol{H}^T_k\left(\boldsymbol{R} + \boldsymbol{H}_k\boldsymbol{P}^-_k\boldsymbol{H}^T_k\right)^{-1} \tag{7}$$

$$\boldsymbol{P}^+_k = \left(\boldsymbol{I} - \boldsymbol{K}_k\boldsymbol{H}_k\right)\boldsymbol{P}^-_k \tag{8}$$

$$\tilde{\boldsymbol{y}}_k = \boldsymbol{z}_k - \boldsymbol{h}\left(\hat{\boldsymbol{x}}^-_k,\boldsymbol{u}_k\right) \tag{9}$$

$$\hat{\boldsymbol{x}}^+_k = \hat{\boldsymbol{x}}^-_k + \boldsymbol{K}_k\tilde{\boldsymbol{y}}_k \; . \tag{10}$$

2.1.2 Estimation of blade-effective wind speeds

We apply the EKF theory to the estimation of blade-effective wind speeds, considering blades as rotating sensors whose bending moments are measured. One estimation is performed for each blade b, as shown in the block diagram of Fig. 1.

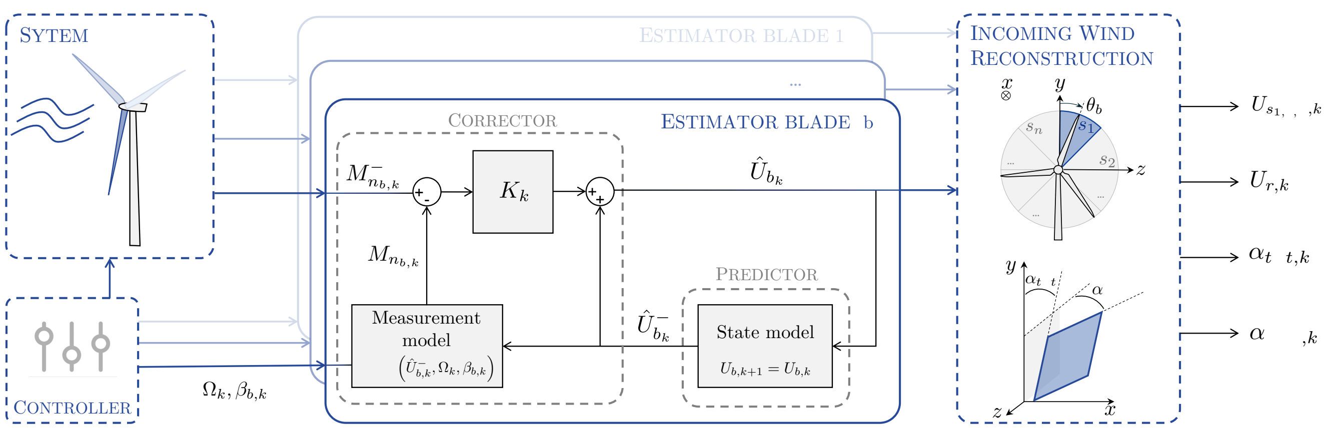

Figure 1. Block diagram of the blade load-based estimator relying on the BEM as internal model and on an extended Kalman filter as an estimator, each blade has its own estimator. The blade-effective wind speeds are mapped to the fixed frame in the wind reconstruction block.

https://doi.org/10.5194/wes-2024-56
Preprint. Discussion started: 15 May 2024

Control input: The control input vector $\boldsymbol{u}$ consists in the rotation speed of the turbine and the blade pitch angle

$$\boldsymbol{u}_k = [\Omega_k, \beta_{b,k}]. \tag{11}$$

State: The variable to be estimated is the blade-effective wind speed, U_b, which is an input to the wind turbine blade system. To match the EKF formalism, we model this input as a state and do not explicitly model the internal states of the system. The one-dimensional state vector therefore writes

$$x_k = U_{b,k}\ . \tag{12}$$

State function: The state evolution is modeled as a random walk with process noise w:

$$U_{b,k} = f(U_{b,k-1}) + w_{k-1} = U_{b,k-1} + w_{k-1}\ . \tag{13}$$

Considering a random walk is equivalent to assuming that the estimated state is a bias, because the expected value is a constant. Using a random walk to model the evolution of the state is thus a simplification in this case, as the blade-effective wind speed is expected to be periodic with a 1P component. A model representation accounting for the 1P-periodicity of the blade-effective wind speed as the one proposed in van Vondelen et al. (2023a) would better represent the system dynamics. Yet, the random walk was successfully used in the context of blade-effective wind speed estimation in Bottasso et al. (2018) and Brandetti et al. (2023), because the 1P variations are slow compared to the estimation time-step and can thus be captured.

Measurement function: The state is estimated based on the measurements of the blade out-of-plane bending moments, M_{n_b}. We model the system using the BEM theory, hence the nonlinear output equation is

$$M_{n_{b,k}} = h\left(U_{b,k}\ ,\ [\Omega_k, \beta_{b,k}]\right) + v_k \tag{14}$$

$$\quad = \mathrm{BEM}\left(U_{b,k}\ ,\ [\Omega_k, \beta_{b,k}]\right) + v_k\ . \tag{15}$$

Note that the original version of the BEM theory is based on the conservation of momentum in a stream tube flowing through the rotor (Hansen, 2015). Therefore, it runs under the assumption of rotor-effective quantities. Appendix A shows how the BEM is used to return individual blade loads from blade-effective velocities.

Another key assumption of the classical BEM theory, which we further refer to as static BEM, is that the wake is fully developed and that the induction of the rotor is then (quasi) steady (Hansen, 2015). In Sec. 4.4, we will show how this BEM model can be modified to account for the induction changes generated by the pitch control strategies considered in this paper.

Jacobian matrices: The expression of the Jacobian matrix for the state function is trivial: $F_k = 1$.

As the BEM is an iterative method (see Appendix A), an analytical expression of the Jacobian matrix for the measurement function cannot be provided. We therefore numerically compute it using central finite differences, with ΔU a constant value tuned manually, following

$$H_k = \frac{h(\hat{U}_{b_k}^{+} + \Delta U, [\Omega_k, \beta_{b,k}]) - h(\hat{U}_{b_k}^{+} - \Delta U, [\Omega_k, \beta_{b,k}])}{2\Delta U}\ .$$

https://doi.org/10.5194/wes-2024-56
Preprint. Discussion started: 15 May 2024

Open Access WIND ENERGY SCIENCE DISCUSSIONS

Note that this procedure requires two more BEM evaluations. Opting for forward finite differences, for example, could save one evaluation if computational time was to become an issue.

2.1.3 Reconstruction of the incoming wind

The estimator described above allows the estimation of the blade-effective wind speeds, that are naturally expressed in the blade rotating frame. They are further manipulated to provide information about the incoming flow in the fixed frame. We also want the information to be provided at a local scale, in order to capture turbulent and shear patterns in the wind. The rotor is then divided into a chosen number of sectors, n_S, and we map the blade-effective wind speeds to the sector-effective wind speeds (see Fig. 1). A sector-effective wind speed U_s is the mean blade-effective wind speed seen by the blade as it traveled across a sector s. A sector-effective wind speed is updated every time a blade leaves that sector, i.e. at a 3P frequency. The update procedure is formally given in Appendix B. At every instant, the rotor-effective wind speed can then be computed as the average velocity of the n_S sectors.

The wind field can also be synthesized as a sheared plane (see Fig. 1). This provides a representation of the shear present in the atmospheric boundary layer through a tilting shear coefficient α_{tilt}, but also gust- or wake-generated shear in the yaw direction α_{yaw}. The least square approximation is used to find the expression of the plane best fitting the sector-effective wind speeds, assuming that the latter account for the wind speed at $r = 2R/3$. The target expression for the velocity field writes

$$U(y,z) = U_r + \alpha_{\text{tilt}}\, y + \alpha_{\text{yaw}}\, z, \tag{16}$$

with y the vertical direction and z the transverse one.

2.2 Simulation environment

The blade load-based estimator is verified numerically. What we consider as the true measurements of the out-of-plane bending moments are provided by LES performed with an in-house wind turbine simulation environment (Chatelain et al., 2017; Balty et al., 2020; Coquelet et al., 2022). The latter relies on a Vortex Particle-Mesh method (Chatelain et al., 2013) in which wind turbine blades are modeled by Immersed Lifting Lines (Caprace et al., 2019). The code is coupled to the multi-body-system solver ROBOTRAN that handles the dynamics of the rigid rotor (Docquier et al., 2013). Turbulence is injected at the inflow using Mann boxes (Mann, 1998). Wind shear can be modeled at the inflow through the following exponential law:

$$\frac{U(y)}{U_{\text{hub}}} = \left(\frac{y}{H_{\text{hub}}}\right)^{\alpha}, \tag{17}$$

where y is the vertical elevation from the ground, H_{hub} and U_{hub} are the hub height and velocity respectively, and α is the shear coefficient.

3 Validation of the estimator for a single turbine in turbulent flows with no shear

In this section, the estimator is validated for an isolated turbine operating in turbulent wind. The numerical setup is first presented, the results are then discussed.

3.1 Numerical setup

The estimator is validated using the NREL 5MW (Jonkman et al., 2009) wind turbine, characterized by a rotor diameter $D = 126$ m, a rated wind speed of 11.4 m/s and a rated rotor speed of 12.1 rpm. For this validation study, we consider wind speeds of 5 m/s, 9 m/s and 14 m/s and turbulence intensity (TI) of 6%, 10% and 15%, hence 9 wind cases are considered. Shear is not present in these simulations and no controller is active: the turbine operates at a prescribed rotation speed and collective pitch angle following Jonkman et al. (2009). The boundary conditions are inflow-outflow in the streamwise direction, x, and unbounded in the vertical, y, and transverse, z, directions. The extent of the computational domain is $8D \times 4D \times 4D$ with a $D/64$ spatial resolution.

3.2 Results

The rotor is discretized into 8 sectors, providing an intermediate spatial resolution in the wind speed estimates. Figure 2 shows the estimation of the sector-effective wind speed (only one sector is shown for the sake of conciseness), the rotor-effective wind speed, and the tilt and yaw shear coefficients. In order to allow for an unambiguous definition of the freestream quantities, an adjunct LES in which no turbine is present is also performed for each case. The estimated rotor and sector quantities can then be assessed by comparing them to the values recovered from this adjunct LES.

The temporal evolution of the sector-effective and rotor-effective wind speeds appears well captured across all simulations. The same global remarks hold for the shear coefficients. As expected, the estimated signals present steps, as a sector velocity is only updated when a blade leaves a sector. This update procedure is also responsible for the delay between the estimated velocities and the reference velocities. One can also notice that the estimates tend to deteriorate as the reference velocity decreases, this is discussed hereunder.

Quantification of the estimator performances is done for the 9 wind condition cases using the following indicators, with N_k the number of time steps:

$$\epsilon_{U_r}^{\text{abs}}\,[\%] = \frac{1}{N_k}\sum_k \frac{|U_{r,k} - U_{r,k}^{\text{LES}}|}{U_{\text{ref}}}\,, \tag{18}$$

$$\epsilon_{U_s}^{\text{abs}}\,[\%] = \frac{1}{n_S N_k}\sum_{s,k} \frac{|U_{s,k} - U_{s,k}^{\text{LES}}|}{U_{\text{ref}}}\,, \tag{19}$$

$$\epsilon_{U_s}\,[\%] = \frac{1}{n_S N_k}\sum_{s,k} \frac{U_{s,k} - U_{s,k}^{\text{LES}}}{U_{\text{ref}}}\,, \tag{20}$$

$$\epsilon_{\alpha_{\text{yaw}}}[\%] = \frac{1}{N_k}\sum_k \frac{|\alpha_{\text{yaw},k} - \alpha_{h,k}^{\text{LES}}|}{\max_k |\alpha_{\text{yaw},k}^{\text{LES}}|}\,, \tag{21}$$

$$\epsilon_{\alpha_{\text{tilt}}}[\%] = \frac{1}{N_k}\sum_k \frac{|\alpha_{\text{tilt},k} - \alpha_{h,k}^{\text{LES}}|}{\max_k |\alpha_{\text{tilt},k}^{\text{LES}}|}\,. \tag{22}$$

https://doi.org/10.5194/wes-2024-56
Preprint. Discussion started: 15 May 2024

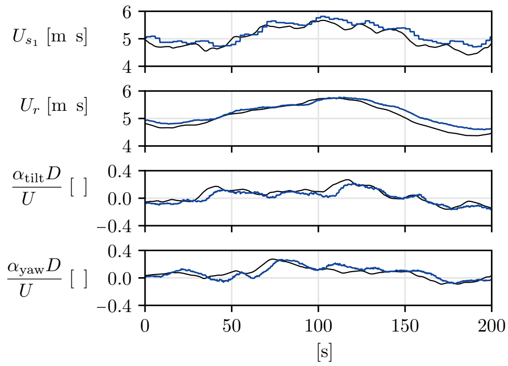

(a) $U_{\mathrm{ref}} = 5$ m/s, $\Omega_{\mathrm{rot}} = 7.5$ rpm, $\beta = 0^{\mathrm{o}}$

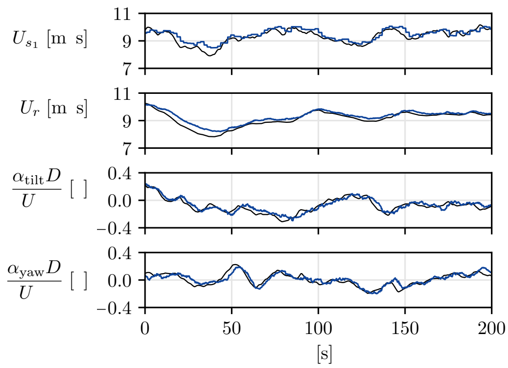

(b) $U_{\mathrm{ref}} = 9$ m/s, $\Omega_{\mathrm{rot}} = 10.3$ rpm, $\beta = 0^{\mathrm{o}}$

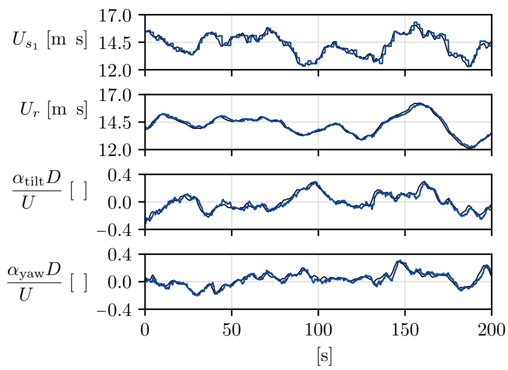

(c) $U_{\mathrm{ref}} = 14$ m/s, $\Omega_{\mathrm{rot}} = 12.1$ rpm, $\beta = 8.7^{\mathrm{o}}$

Figure 2. Estimated wind characteristics (sector-effective wind speed, rotor-effective wind speed, shear coefficients) at three wind speeds with $\mathrm{TI} = 10\%$: LES-recovered references (black) and estimated values (blue).

First, a degradation of error metrics at higher TIs is observed in Table 1. We attribute this to the inherent spatial filtering introduced by the blade-as-a-sensor approach. This hinders the ability of the estimator to sense local wind fluctuations and the effect of this limitation increases with increasing TI. Adapting the process noise Q based on the mean TI could be envisioned.

https://doi.org/10.5194/wes-2024-56
Preprint. Discussion started: 15 May 2024

WIND ENERGY SCIENCE DISCUSSIONS

U_{ref} [m/s]	5			9			15		
TI [%]	6	10	15	6	10	15	6	10	15
$\epsilon^{\text{abs}}_{U_r}$ [%]	2.2	2.6	3.6	1.7	3.1	3.1	0.5	0.8	1.7
$\epsilon^{\text{abs}}_{U_s}$ [%]	2.5	3.4	4.9	2.1	4.6	4.5	1.0	1.8	3.0
ϵ_{U_s} [%]	2.3	2.5	3.3	1.4	2.5	1.7	0.2	0.3	0.5
ϵ_{α_h} [%]	6.1	7.9	6.6	5.8	14.9	6.7	4.2	4.9	4.9
ϵ_{α_v} [%]	8.0	7.9	7.7	7.6	9.5	7.6	5.2	5.1	5.6

Table 1. Relative errors for the estimation of the rotor-effective wind speed, the sector-effective wind speed and the shear coefficients for the 9 validation cases.

Regarding the estimation of the rotor-effective velocity, the relative absolute error remains under 4%, while for the sector-effective velocities, it remains under 5%. These errors are similar to those reported in Bottasso et al. (2018). We also verify whether a bias is present in the estimation by computing ϵ_{U_s}. Table 1 shows that a bias around 0.3% is present for $U_{\text{ref}} = 15$ m/s and it increases to become of the order of $2-2.5\%$ for $U_{\text{ref}} = 5$ m/s. Kalman filters require a internal model linking the system states and observations. If the model deviates from the actual system, then the estimation will be biased. In this case, the LES is considered as the real system in which the estimator is tested, while the internal model of the estimator is the BEM. It is known from the literature that the one-dimensional momentum theory from which the BEM is derived breaks down at low wind speeds as the rotor is heavily loaded (Hansen, 2015). A mismatch therefore appears between the internal model of the estimator, the BEM, and the actual system, the LES, as the wind speed decreases.

While the absolute level of the forces is higher in the LES than in the BEM, hence the positive bias in the estimation, the dynamical variations of the system are well captured (see Fig. 2). The estimator thus entails a great perception of the temporal and local changes in wind speed, which is what is of most interest for the control purposes that are targeted in this paper. Would the bias still be an issue, a bias-aware EKF could be used, as suggested by Drécourt et al. (2006). A common practice is to augment the state vector of the original problem with the bias (Friedland, 1969). The EKF therefore estimates both the state and the bias, as done in the work of Pamososuryo et al. (2023) in the context of wind turbine control.

4 Robustness of the estimator to active pitch control strategies

While the previous section has focused on validating the estimator, this section aims at testing it in more realistic wind conditions and when controllers are active on the turbine. The choice of the study cases is motivated hereunder.

https://doi.org/10.5194/wes-2024-56
Preprint. Discussion started: 15 May 2024

Open Access WIND ENERGY SCIENCE DISCUSSIONS

4.1 Controllers

The estimator presented here relies on blade loads and operating parameters. Both are influenced by the controller that is active on the wind turbine. In this section, we verify that the estimator is robust to the chosen control strategy. To do so, we propose simulations in which the three following pitch control strategies are considered: individual pitch control for load alleviation, individual pitch control for wake mixing and collective pitch control for wake mixing. The implementation of these controllers is presented hereafter.

A Baseline controller is active in all cases and serves as a comparison for the other cases. It is a classical implementation of a variable-speed, variable-pitch controller (Jonkman et al., 2009). It relies on generator torque control, maximizing the power captured below the rated wind speed, and Collective Pitch Control (CPC), regulating the collective pitch angle β_{coll} to maintain nominal power production above the rated wind speed.

For the controllers relying on individual pitch actions, the Coleman transform is used to map fixed-frame pitch commands to rotating-frame ones (Bossanyi, 2003). The individual blade pitch angles $\beta_{1,2,3}$ are retrieved from the fixed-frame pitch angles, β_{tilt} and β_{yaw}, and the collective pitch angle β_{coll}, based on the inverse Coleman transform:

$$\begin{bmatrix} \beta_1 \\ \beta_2 \\ \beta_3 \end{bmatrix} = \begin{bmatrix} 1 & \cos\theta & \sin\theta \\ 1 & \cos\left(\theta - \frac{2\pi}{3}\right) & \sin\left(\theta - \frac{2\pi}{3}\right) \\ 1 & \cos\left(\theta + \frac{2\pi}{3}\right) & \sin\left(\theta + \frac{2\pi}{3}\right) \end{bmatrix} \begin{bmatrix} \beta_{\text{coll}} \\ \beta_{\text{tilt}} \\ \beta_{\text{yaw}} \end{bmatrix},$$

where θ is the azimuthal position of the first blade ($\theta = 0$ when the blade is pointing upward).

The IPC-based load alleviation controller, further referred to as IPC, consists of two PI controllers, one for the yaw axis and one for the tilt axis. They compute the fixed-frame pitch commands $\beta_{\text{tilt,yaw}}$ bringing the fixed-frame loads $M_{\text{tilt,yaw}}$ to zero, in the fashion of Bossanyi (2003). More details on this specific implementation can be found in Coquelet et al. (2020).

The IPC-based wake mixing controller, further referred to as Helix, is implemented as an open-loop control strategy (Frederik et al., 2020). It imposes sinusoidal variations of the fixed-frame pitch angles, namely $\beta_{\text{tilt}} = A\sin(2\pi f_p\, t)$ and $\beta_{\text{yaw}} = A\cos(2\pi f_p\, t)$. The frequency f_p is defined by the Strouhal number $St = f_p D/U_{\text{ref}}$, based on the rotor diameter D and the wind speed U_{ref}. The pitch actuation generates variations of the tilt and yaw moments, eventually forcing the wake to displace laterally (see Fig. 3) and to propagate downstream as a helix, hence the name.

The CPC-based wake mixing controller generates a pulsing pattern in the wake (see Fig. 3) by periodically changing the thrust force of the rotor. The position of the wake is not impacted, but its intensity and expansion change over time as a result of the changes in induction. We further refer to this strategy as the Pulse. It is implemented as a superimposition of low-frequency harmonic oscillations onto the collective pitch angle β_{coll} computed by the baseline controller. The pitch angle evolution is thus dictated by

$$\beta_1 = \beta_2 = \beta_3 = \beta_{\text{coll}} + A\sin\left(2\pi St \frac{U_{\text{ref}}\, t}{D}\right). \tag{23}$$

https://doi.org/10.5194/wes-2024-56
Preprint. Discussion started: 15 May 2024

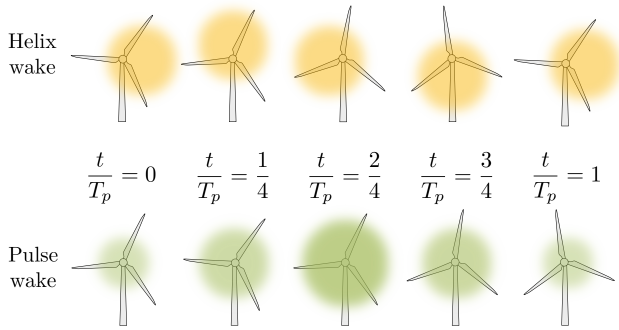

Figure 3. Simplified representation and description, over a period T_p, of the Helix (yellow) and Pulse (green) wakes impinging on a downstream wind turbine. The colored zone schematically represents the wake deficit, the opacity reflects its intensity while the radius reflects its expansion.

4.2 Numerical set-up

We perform the LES of a pair of in-line NREL 5MW turbines with a $5D$ spacing, such that the estimator can be tested on a freestream turbine but also on a waked turbine. The inflow wind is sheared and turbulent, in order to represent atmospheric boundary layer flows. The wind speed at hub height $U_{\text{ref}} = 9$ m/s, the shear coefficient is $\alpha = 0.2$ and the turbulence intensity at hub height is equal to 6%. The boundary conditions are inflow-outflow in the streamwise direction x, slip wall in the vertical direction y, and periodic in the transverse direction z. The numerical domain has dimensions of $12D \times 3D \times 8D$ and the spatial resolution is $D/32$. The four aforementioned controllers are tested for the upstream turbine: Baseline, IPC, Pulse, and Helix. We opt for commonly used parameters for both the Helix and the Pulse (Frederik et al., 2020; Munters and Meyers, 2018): $St = 0.25$ and $A = 2.5^{\text{o}}$. The downstream turbine is always operated using the Baseline controller.

The wind speed estimation for both the upstream and the downstream turbine is presented hereunder. For the upstream one, the reference velocities is defined as the velocity from a slice located at the rotor position when the rotor is not present (Fig. 4(b)). When it comes to the downstream turbine, the reference velocities are accordingly retrieved from simulations of each control case in which only the first turbine is present (Fig. 4(c)).

4.3 Impact of the control strategy on operating parameters and measured loads

Figure 5 shows the impact of the controller on the operating parameters and the out-of-plane moments. The Baseline case shows that, if the pitch is equal for all blades, the effect of shear and turbulence generates 1P oscillations (period T_{rot}) on the blade bending moments.

When IPC is used, the changes in wind speed perceived by the blade as it rotates are compensated by the pitch angles. These vary individually at the 1P frequency, the amplitude of the actuation varies with time as the controller operates in closed loop.

https://doi.org/10.5194/wes-2024-56
Preprint. Discussion started: 15 May 2024

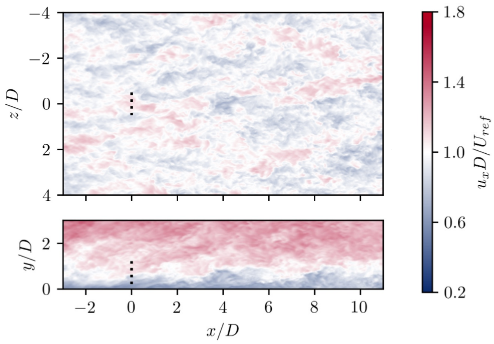

(a) Simulation used to compute reference wind speeds for the upstream turbine.

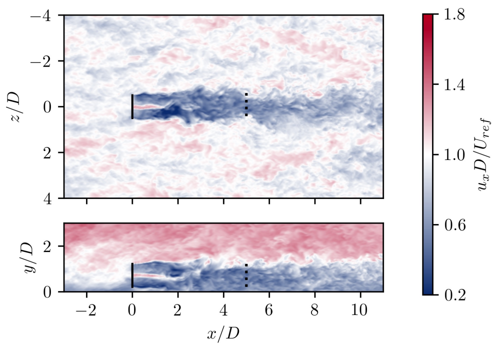

(b) Simulation used to compute reference wind speeds for the downstream turbine.

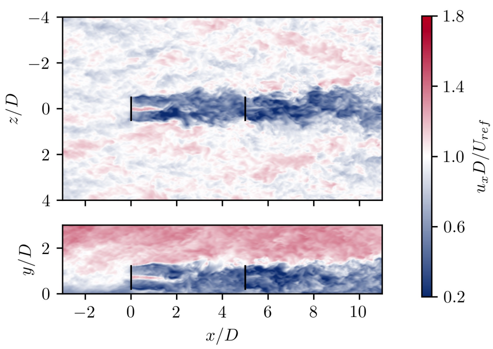

(c) Simulation used to retrieve the operating parameters and bending moments on the two turbines.

Figure 4. Horizontal and vertical slices of the instantaneous streamwise velocity field used as reference wind speeds to verify it for the first (a) and second (b) turbines, and simulation used to retrieve bending moments to feed the estimator (c). Only the Baseline control case is shown.

https://doi.org/10.5194/wes-2024-56
Preprint. Discussion started: 15 May 2024

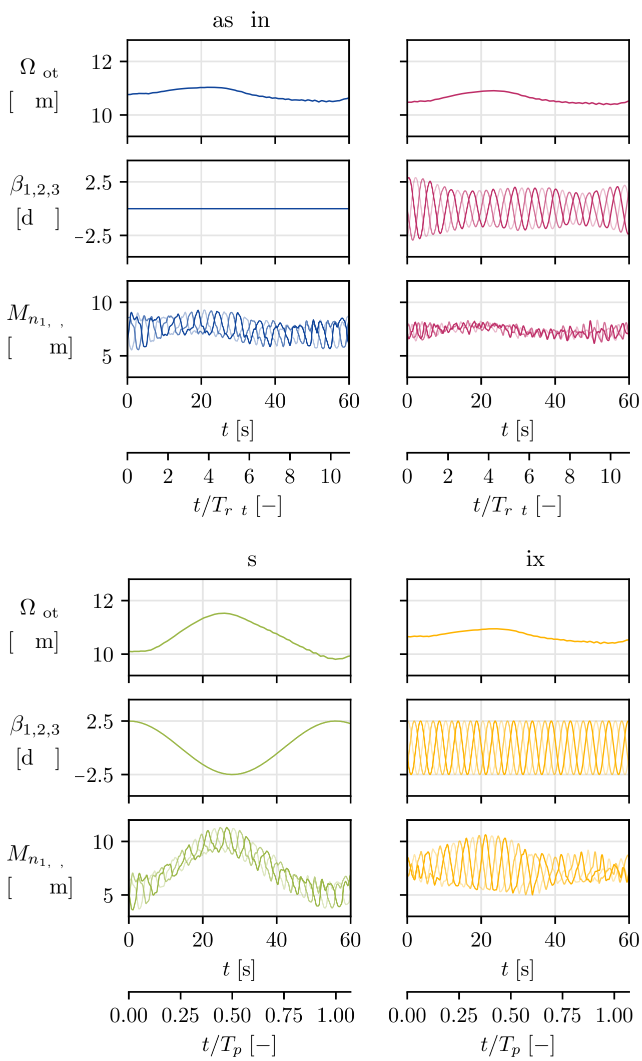

Figure 5. Effect of the control strategy on rotation speed, blade pitch angles, and out-of-plane bending moment. One color shade is used for each blade. The time axis is given in seconds and rotation periods T_{rot} for the Baseline and IPC controllers as the dominant effects are observed at 1P in those cases. For the Pulse and the Helix, time is made dimensionless using the actuation period T_p.

For the Pulse, all blades are pitched at the same angle. Given the Strouhal number of 0.25, the actuation period T_p is about ten times the rotation period. The amplitude of the pitch oscillations is constant as the strategy is open loop. The mean value of the out-of-plane moments is marked by this periodicity and displays the changes in rotor induction.

For the Helix case, it comes from the Coleman transform that the pitching frequency is $1/T_{\text{rot}} + 1/T_p$ (see Frederik et al. (2020) for derivation) with a constant amplitude. This does not impact the mean value of the bending moments, as the individual

https://doi.org/10.5194/wes-2024-56
Preprint. Discussion started: 15 May 2024

pitch action is performed in a three-phase manner, with a 120º offset between each blade. Rather, the effect is also visible on the amplitude of the bending moments, which is sometimes increased (around $t = 20$ s in Fig. 5) and sometimes decreased (around $t = 50$ s in Fig. 5). The effect is better understood looking at tilt and yaw moments, as those become quadrature phase sinusoidal signals with a $1/T_p$ frequency.

This section has highlighted how the control strategies considered in this work impact the state of the turbine, i.e. its operating parameters and the loads it experiences. This further motivates the need to verify the robustness of the blade load-based estimator to the pitch control strategy active on the turbine. It also points at verifying the accuracy of the inner model used in the estimator, i.e. the BEM, in scenarios that involve dynamic actuation.

4.4 Handling effects of dynamic actuation in the BEM

In the current formulation of the estimator, the internal model relies on the BEM theory. As discussed before, the standard BEM behaves as a static mapping between the operating parameters of the turbine and the wind speed, and the forces exerted on the blades. This comes from the assumption of the BEM that the wake is fully developed, which underlies that the induction of the blades and thus the induced velocities around them are (quasi) steady. Yet the Pulse and the Helix inherently generate periodic variations of the induction, hence the wake is never fully developed. Through the collective pitch actuation, the Pulse changes the induction of the entire rotor. When it comes to the Helix, the individual pitch actuation changes the local induction of each blade. A time delay therefore exists before equilibrium is reached between the induction factors and the aerodynamic loads. In order to account for it, we propose to make use of a dynamic formulation for the BEM, based on the work of Snel and Schepers (1995). Appendix A presents how the quasi-steady normal a and tangential a' induction factors are computed. From these induction factors, the quasi-steady induced velocities, normal w_n and tangential w_t, are recovered as $\mathbf{w}_{\text{qs}} = [w_n, w_t] = [aU_0, a'\Omega_{\text{rot}} r]$, where U_0 is the infinite upstream velocity and r is the local radius of the considered blade section (see Fig. A1).

Following Snel and Schepers (1995), the induced velocities are filtered with the following first-order differential equations

$$\mathbf{w}_{\text{int}} + \tau_1 \frac{\mathrm{d}\mathbf{w}_{\text{int}}}{\mathrm{d}t} = \mathbf{w}_{\text{qs}} + k_1\, \tau_1 \frac{\mathbf{w}_{\text{qs}}}{\mathrm{d}t}\,, \tag{24}$$

$$\mathbf{w} + \tau_2 \frac{\mathrm{d}\mathbf{w}}{\mathrm{d}t} = \mathbf{w}_{\text{int}}, \tag{25}$$

where $\mathbf{w}_{\text{int}}$ is a working variable, $k_1 = 0.6$ is a constant and τ_1 and τ_2 are time constants.

The corrected induction factors are retrieved from the corrected induced velocities $\mathbf{w} = [w_n, w_t]$ following

$$[a,\, a'] = [w_n/U_0,\; w_t/(\Omega_{\text{rot}}\, r)]. \tag{26}$$

We further refer to the BEM without dynamic effects as the static BEM and to the one enhanced with dynamic effects as the dynamic BEM. The tunable time constants τ_1 and τ_2 for the dynamic BEM are calibrated against LES data. To do so, we perform the simulation of the NREL 5MW in uniform inflow with no shear at $U_{\text{ref}} = 9$ m/s when the Pulse and the Helix are active. The turbine rotation speed and blade pitch angles computed by the controller are retrieved from the LES and fed to the

https://doi.org/10.5194/wes-2024-56
Preprint. Discussion started: 15 May 2024

static and dynamic BEM. We recall that the Immersed Lifting Line method used to compute aerodynamic loads in the LES intrinsically accounts for dynamic effects in the induction and is thus the reference.

Based on the analytical expression provided in Hansen (2015), we propose that:

$$\tau_1 = \frac{1}{7(1-1.3a)}\frac{1}{f_{\text{pitch}}}, \tag{27}$$

$$\tau_2 = \left(0.39 - 0.26\left(\frac{r}{R}\right)^2\right)\tau_1, \tag{28}$$

with R, the rotor radius. TSR being the tip speed ratio, we recall that the pitching frequency of the blade f_{pitch} is

$$f_{\text{pitch}}^{\text{Pulse}} = f_p = St\,\frac{U_{\text{ref}}}{D} \tag{29}$$

$$f_{\text{pitch}}^{\text{Helix}} = f_{\text{rot}} + f_p = \left(\frac{\text{TSR}}{\pi} + St\right)\frac{U_{\text{ref}}}{D}. \tag{30}$$

Figure 6 compares, over one period T_p, the BEM values with those provided by the LES for the local induction and the out-of-plane bending moment. It shows that, with the static BEM, the axial induction is in direct phase opposition with the pitch angle. It behaves as if, as soon as the pitch angle increases, the induced velocities are reduced. When considering the dynamic effects, a certain delay appears, which is different for the Pulse and the Helix as the tuning of the time constants has shown. Not taking the delays into account leads to poor evaluation of the angle of attack, which eventually leads to inaccurate loads. Including dynamic effects in the BEM therefore increases the accuracy of the internal model of the estimator, which should improve the quality of the estimate provided by the EKF.

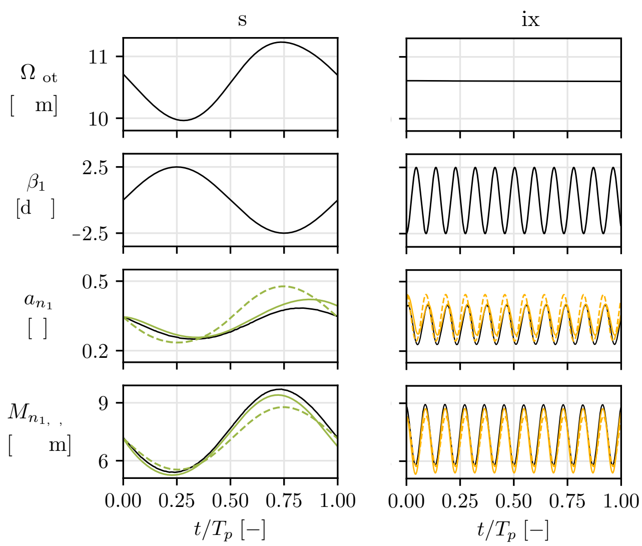

Figure 6. Comparison of LES (solid black), static BEM (dashed colored) and dynamic BEM (solid colored) in the evaluation of the local forces acting on the airfoil located at $r/R = 3/4$ for the NREL 5MW operated in uniform flow with $U_{\text{ref}} = 9$ m/s.

https://doi.org/10.5194/wes-2024-56
Preprint. Discussion started: 15 May 2024

4.5 Results for the upstream turbine

We divide the rotor into four sectors ($n_S = 4$) placed as a cross, which leads to a top, right, bottom, and left sector. This allows us to capture the effects of shear thanks to the top-bottom differences and the effects of gust or wake impingement through the left-right imbalances. We first comment the results of the estimator in its original formulation, i.e. using static BEM. Time series of the rotor-effective and sector-effective wind speeds are provided in Fig. 7, along with their Power Spectral Density (PSD).

When it comes to the rotor-effective wind speed, the estimations are almost identical for the Baseline, IPC and Helix cases. When the Pulse is active on the turbine, oscillations appear in the wind speed estimate at the Pulse frequency. For the sector-effective wind speed, these oscillations are present not only for the Pulse but also for the Helix.

This highlights that neglecting the dynamic effects in the internal model of the system, as it is done with the look-up table approaches in Bottasso et al. (2018), Liu et al. (2021) or Liu et al. (2022), is inadequate for the considered application. When the static BEM is used, the expected measurement provided by the internal model in the EKF is not accurate. There is a mismatch with the actual measurement, and the wind speed estimate is wrongfully corrected in the correction step. For the Pulse, this leads to periodic oscillations of both the rotor-effective wind speed and the sector-effective wind speed at the actuation frequency $1/T_p$. With the Helix control, the changes of induction are performed individually at each blade in a three-phase manner, with a 120° offset between each blade. The inaccurate oscillations therefore appear on the blade-effective wind speeds, but they cancel out at the rotor scale.

Figure 7 presents the result of the estimators once dynamics is taken into account in the internal BEM model. The estimates are now identical whatever the control strategy active on the turbine: the adapted estimator is robust to the control strategy. The capacities of the estimator described in Sec. 3 and demonstrated by several studies in the literature are then retrieved. The estimator is able to recover the higher velocities in the top sector, the intermediate ones in the left and right sectors, and the lower ones in the bottom sector. It is thus able to capture turbulence, shear, gusts, etc. The estimation errors are reported in Table 2 and are close to 5%.

	Baseline	IPC	Pulse	Helix
$\epsilon^{\text{abs}}_{U_r}$ [%]	5.4	5	5.2	5.1
$\epsilon^{\text{abs}}_{U_s}$ [%]	5.7	5.3	5.5	5.5
ϵ_{U_s} [%]	5.5	5.0	5.3	5.3

Table 2. Wind speed estimation errors for the upstream turbine.

The overestimation bias discussed in Sec. 3 is also observed, yet it is around 5% here, while it was around $1.5-2\%$ in the validation case at the same 9 m/s wind speed. We attribute this increase in bias to the set-up used for the simulations. Indeed, to maintain limited computational costs for the LES, the spatial resolution used in these runs is coarsen to $D/32$, while the resolution was twice finer in Sec. 3. It is known that the forces computed by the LES increase when the resolution

https://doi.org/10.5194/wes-2024-56
Preprint. Discussion started: 15 May 2024

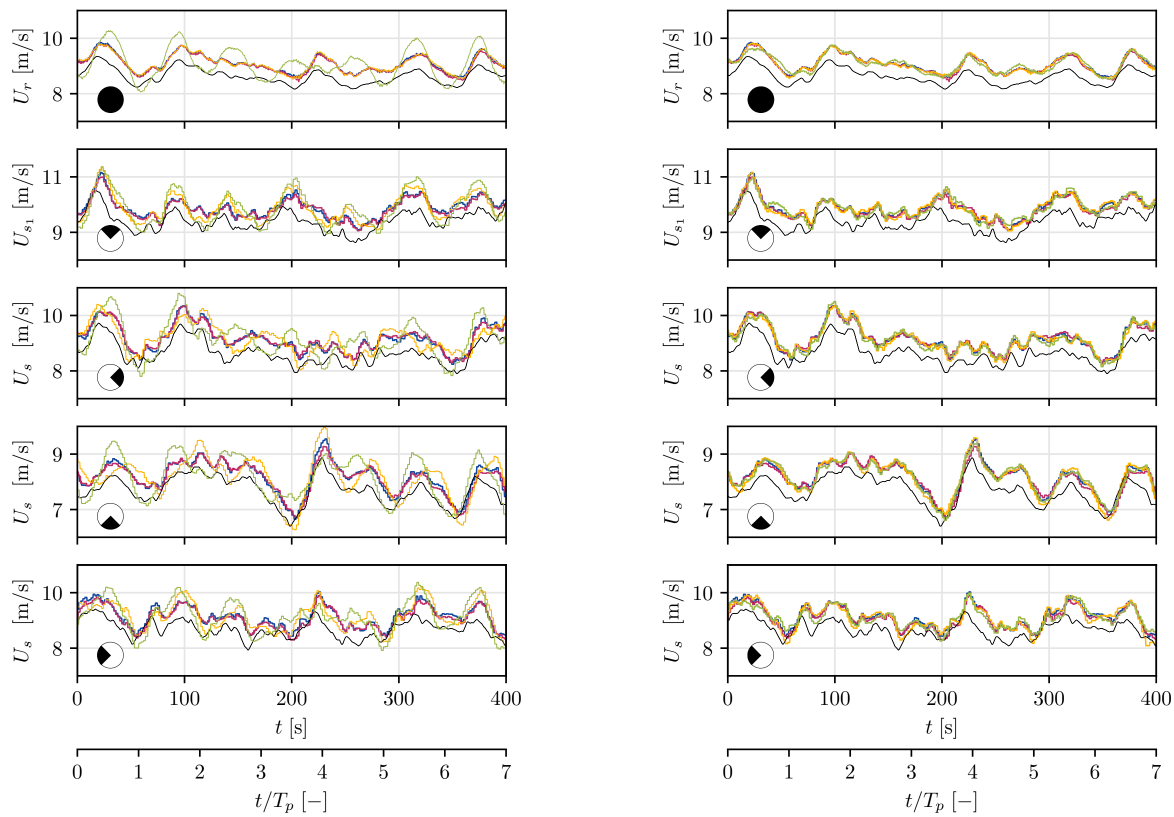

(a) Time series of the estimated wind speeds using static BEM.

(b) Time series of the estimated wind speeds using dynamic BEM.

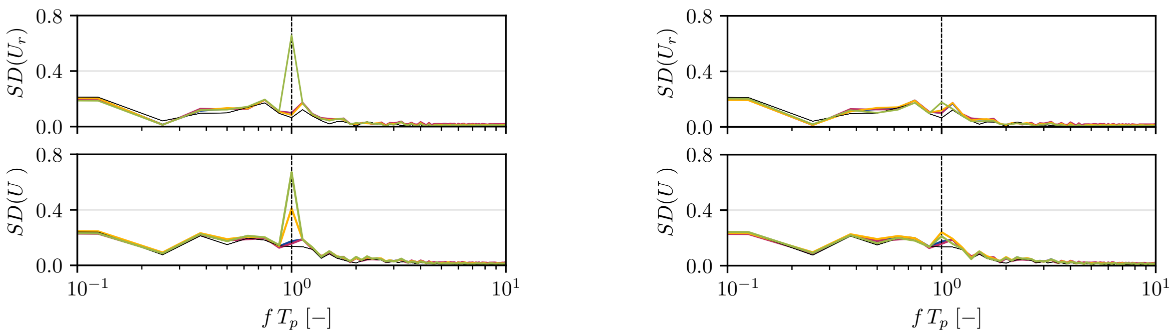

(c) Power spectral density of the time series using static BEM.

(d) Power spectral density of the time series using dynamic BEM.

Figure 7. Wind speed estimation on the upstream turbine using a static (left) and dynamic (right) BEM as the internal model in the EKF. Reference velocities (black) are extracted from the LES. The wind speeds are estimated by the upstream turbine which is operated with four different control strategies: Baseline (blue), IPC (red), Pulse (green) and Helix (yellow).

https://doi.org/10.5194/wes-2024-56
Preprint. Discussion started: 15 May 2024

eawe european academy of wind energy
Open Access WIND ENERGY SCIENCE DISCUSSIONS

decreases due to poor capture of the tip losses (Moens et al., 2018). The mismatches between the internal model (BEM) and the actual system (LES) is higher with the simulations in this section than with those from Sec. 3. In the correction step, the EKF therefore corrects the velocity to a higher value than it should. As suggested before, this could be corrected with bias estimation (Friedland, 1969).

4.6 Results for the downstream turbine

The Pulse and the Helix are wake mixing control strategies, which means that their purpose is to modify the wake. Namely, the Pulse is expected to generate a pulsing sequence in the wake, with alternating zones of lower and higher velocities while the Helix laterally displaces the wake as it propagates downstream (see Fig. 3). In this last section, we want to verify the performances of the estimator in waked flows and its ability to capture the frequency content added to the wake by the Pulse and the Helix.

Figure 8(a) shows that the estimator performs reasonably well in waked conditions, capturing the large-scale changes in the wind. Yet, the estimation somewhat deteriorates compared to the upstream turbine case, as Table 3 reports. Two reasons can be mentioned to support the bigger discrepancies and stem from the inherent characteristics of a wind turbine wake: reduced velocity and higher turbulence. On the one hand, the flow dynamics is harder to capture due to the complexity and randomness of turbulence. The amplitude of the peaks is not fully captured by the estimator, likely also due to the filtering effect of the blade-to-sector conversion. On the other hand, the BEM loses accuracy at lower velocity, hence the bigger bias present in the estimation (6% on average against the 5% for the freestream turbine).

	Baseline	IPC	Pulse	Helix
$\epsilon_{U_r}^{\text{abs}}$ [%]	6.4	6.2	5.8	6.6
$\epsilon_{U_s}^{\text{abs}}$ [%]	7.0	6.9	6.6	7.4
ϵ_{U_s} [%]	6.5	6.4	5.9	6.7

Table 3. Wind speed estimation errors for the downstream turbine. The controller refers to the controller that is active on the upstream turbine. The downstream turbine is always operated with Baseline control. The IPC case is also reported though not shown in Fig. 8.

Figure 8(b) shows that the estimator is able to capture the frequency content added to the wake by the Pulse and the Helix control strategies. Looking back at the time series, the added periodicity can also be observed. It is mostly interesting to notice that the phase at which higher and lower velocity flow parcels are impacting a sector, or the rotor, is properly captured. This is an interesting result from the perspective of applying the Helix or the Pulse to deeper lines of turbines. The downstream turbine could therefore also be actuated with the Helix or the Pulse and synchronize its action with the periodic perturbations already present in the wake, as proposed in van Vondelen et al. (2023a) or Korb et al. (2023).

https://doi.org/10.5194/wes-2024-56
Preprint. Discussion started: 15 May 2024

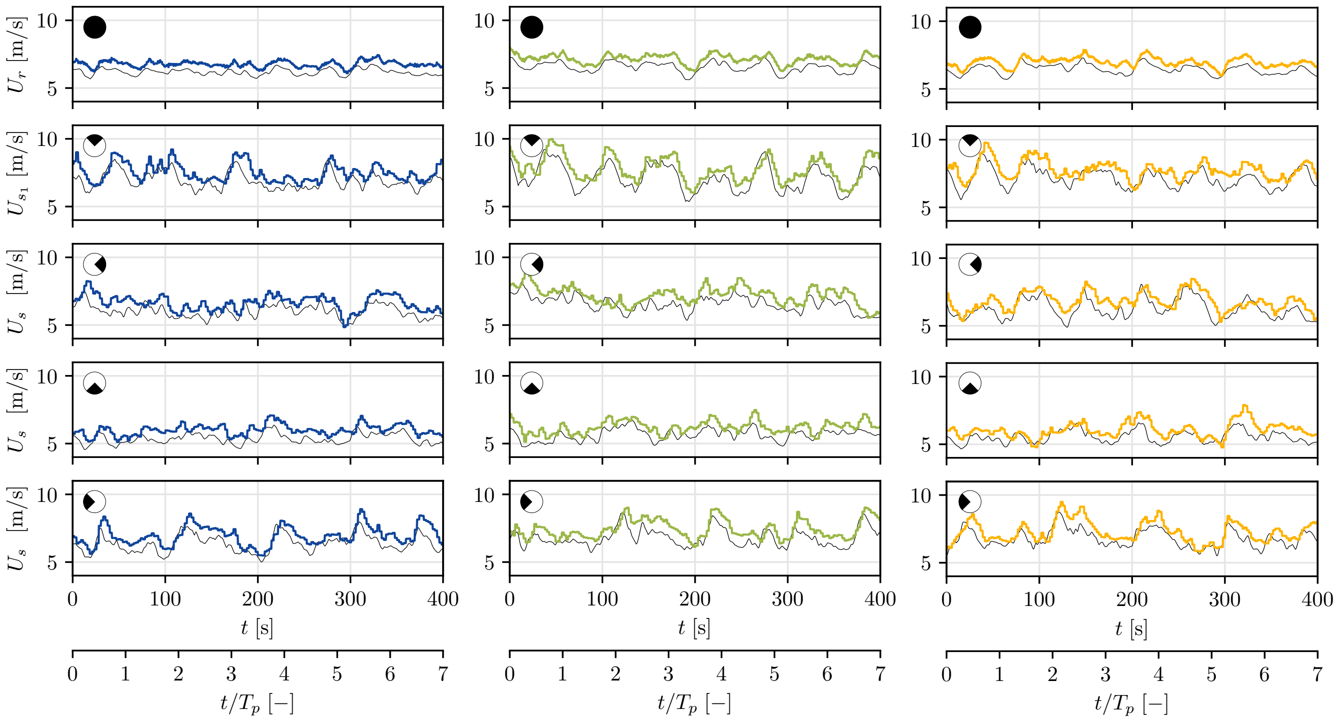

(a) Time series of the estimated wind speeds.

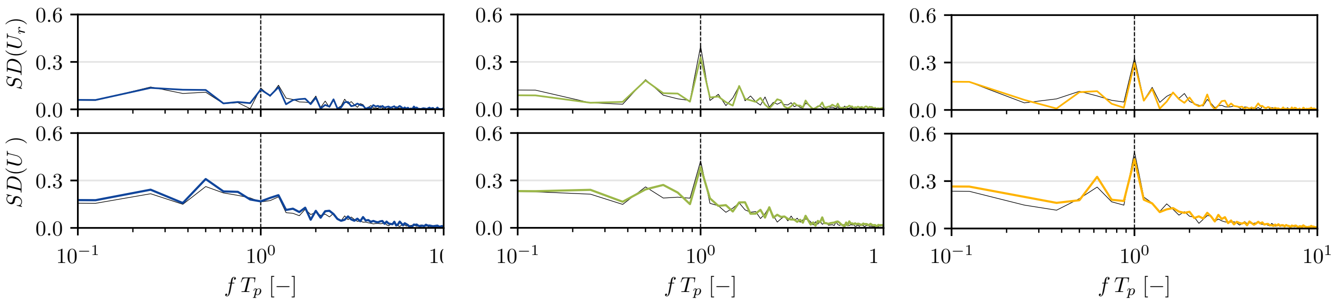

(b) Power spectral density (PSD) of the time series.

Figure 8. Wind speed estimation on the downstream turbine, operated with Baseline control, using a static BEM as internal model in the EKF. Reference velocities (black) are extracted from the LES with the sole upstream turbine operated with four different control strategies: Baseline (blue), Pulse (green) and Helix (yellow).

https://doi.org/10.5194/wes-2024-56
Preprint. Discussion started: 15 May 2024

5 Conclusions

This work assesses the ability of a blade load-based wind speed estimator to accurately sense the characteristics of the incoming wind when both collective and individual pitch control is active at the turbine.

The proposed estimator relies on Extended Kalman filter, whose internal model of the system is based on the BEM theory. We show the need to include dynamic effects in the BEM for the wake mixing cases, as their working principle is to dynamically vary blade induction. Indeed, the static BEM considers an immediate reaction of the blade loads to the pitch actuation, ignoring the unsteady effects in the wake related to the changes in induction. When load alleviation IPC is used, unsteady effects are not generated in the wake, the pitching rather homogenizes the loads experienced by the blades throughout their rotation. The static BEM is therefore not an accurate model when control strategies relying on dynamic changes of induction, as the Pulse and the Helix, are active on the turbine. Including to possibility to add an unsteady correction in that model is the solution we propose to make the EKF robust to the controller active on the turbine. This contribution is essential if the EKF is to be used for state-feedback control, the application targeted for this tool.

A direct follow-up to this work then consists in determining if the precision provided by this estimator is sufficient for control applications. This comes along with including a solution to account for the bias of the estimator, or finding a control formulation in which it is not impacting. For IPC, load alleviation in waked conditions is still challenging and could benefit from explicit information on local wind speeds and global shear coefficients provided by the estimator. For the Pulse and the Helix controllers, sensing the incoming flow is needed for them to be used in a closed-loop manner. This would allow them to optimally phase their dynamic actuation with the dynamics of the incoming flow structures. This refers to the gusts and shear of the atmospheric boundary layer for the upstream turbine and the impinging periodic wakes for downstream turbines.

Appendix A: Blade Element Momentum theory

Algorithm A1 recalls the key steps of the BEM computation and the quantities of interest are illustrated in Fig. A1. The Glauert correction is used for high induction and, when needed dynamic effects can be taken into account (see Sec. 4.4). We refer to Hansen (2015) for more details.

Appendix B: From blade-effective wind speed to sector-effective wind speed

Algorithm B1 formalizes the conversion from blade-effective wind speed to sector-effective wind-speed. The principle is to accumulate information while a blade passes through a sector and to update the sector-effective wind speed when the blade leaves the sector.

https://doi.org/10.5194/wes-2024-56
Preprint. Discussion started: 15 May 2024

WIND ENERGY SCIENCE DISCUSSIONS

Algorithm A1 BEM

for Each blade section **do**

Radial position r, chord c

Initialize induction factors

$a = 0.5, \quad a' = 0.005$

while $a_{\text{new}} - a_{\text{old}} < \text{tol}$ **do**

$a_{\text{old}} = a, \quad a'_{\text{old}} = a'$

Compute angle of attack and relative velocity

$U_n = (1-a)\,u_0, \quad U_t = (1+a')\,\Omega_{\text{rot}} r$

$\phi = \tan^{-1}(U_n/U_t)$

$\alpha = \phi - (\beta + \gamma)$

$U_{\text{rel}} = \sqrt{U_n^2 + U_t^2}$

Retrieve lift and drag coefficients from polar

$C_L = C_L(\alpha), C_D = C_D(\alpha)$

Compute normal and tangential force coefficients

$C_n = C_L \cos\phi + C_D \sin\phi \quad C_t = C_L \sin\phi - C_D \cos\phi$

Compute new induction factors

$$F_{\text{tip}} = \frac{2}{\pi}\arccos\left(\exp\left(-n_B \frac{R-r}{2r\sin\phi}\right)\right)$$

$$F_{\text{hub}} = \frac{2}{\pi}\arccos\left(\exp\left(-n_B \frac{r-R_{\text{hub}}}{2r\sin\phi}\right)\right)$$

$$\sigma = \frac{n_B c}{2\pi r}$$

$$a = \frac{1}{\dfrac{4F\sin^2\phi}{\sigma C_n} + 1}$$

$$a' = \frac{1}{\dfrac{4F\sin\phi\cos\phi}{\sigma C_t} - 1}$$

$a_{\text{new}} = a, \quad a'_{\text{new}} = a'$

end while

Compute local tangential and normal force

$f_n = \frac{1}{2}\rho U_{\text{rel}}^2 c C_n, \quad f_t = \frac{1}{2}\rho U_{\text{rel}}^2 c C_t$

end for

Integrate over span to compute out-of-plane bending moment of blade b

$M_{n,b} = \int_{R_{\text{hub}}}^{R_{\text{tip}}} (r - R_{\text{hub}})\, f_{n,b}\, dr$

https://doi.org/10.5194/wes-2024-56
Preprint. Discussion started: 15 May 2024

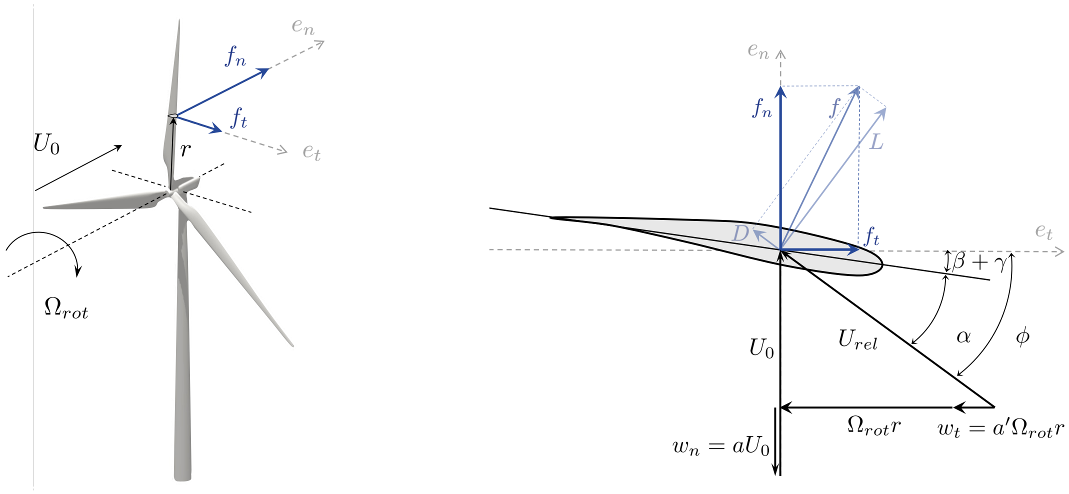

(a) Reference frame for the forces computation

(b) Velocity triangle at a cross-section of the blade

Figure A1. Quantities of interest in the BEM computation

Algorithm B1 Transforming blade-effective wind speeds to sector-effective wind speeds

initialization at time instant $k = 1$

$U_{s,1} = 0 \quad \forall\, s$

$\mathrm{nit}_b = 1 \quad \forall\, b$

$s_{b,1} = \mathrm{integer}\,(\theta_{b,1}/\Delta\theta) \quad \forall\, b$

while estimation is ongoing **do**

$U_{s,k} \leftarrow U_{s,k-1} \quad \forall\, s$

for b in n_B **do**

$s_{b,k} = \mathrm{integer}\,(\theta_{b,k}/\Delta\theta)$

if $s_{b,k} \neq s_{b,k-1}$ **then**

$s^* = s_{b,k-1}$

$U_{s^*,k} \leftarrow \frac{1}{\mathrm{nit}_b} \sum_{\kappa=k-\mathrm{nit}_b}^{k-1} U_{b,\kappa}$

$\mathrm{nit}_b \leftarrow 1$

else

$\mathrm{nit}_b \leftarrow \mathrm{nit}_b + 1$

end if

end for

end while

https://doi.org/10.5194/wes-2024-56
Preprint. Discussion started: 15 May 2024

eawe european academy of wind energy
Open Access
WIND ENERGY SCIENCE
DISCUSSIONS

Author contributions. MC, ML, PC and LB worked at conceptualizing this research and establishing the methodology. MC and ML developed the BEM and EKF software. MC set-up, ran and postprocessed the LES. AV and JWW provided feedback on the methodology. MC prepared the original draft with contribution from all authors, which was then reviewed by all authors. PC, LB and JWW provided funding.

Competing interests. At least one of the (co-)authors is an Associate editor of Wind Energy Science.

Acknowledgements. This project has received funding from the European Research Council under the European Union's Horizon 2020 research and innovation program (grant agreement no. 725627) and from the Université de Mons under the 50/50 PhD funding program. This work is also part of Hollandse Kust Noord wind farm innovation program where CrossWind C.V., Shell, Eneco, Grow and Siemens Gamesa are teaming up; funding for the PhD's and PostDocs was provided by Cross- Wind C.V. and SiemensGamesa.

This research benefited from computational resources made available on the Tier-1 supercomputer of the Fédération Wallonie-Bruxelles, infrastructure funded by the Walloon Region under the grant agreement no. 1117545. Computational resources were also provided by the Consortium des Equipements de Calcul Intensif, funded by the Fonds de la Recherche Scientifique de Belgique under Grant No. 2.5020.11 and by the Walloon Region.

https://doi.org/10.5194/wes-2024-56
Preprint. Discussion started: 15 May 2024

References

Balty, P., Caprace, D.-G., Waucquez, J., Coquelet, M., and Chatelain, P.: Multiphysics simulations of the dynamic and wakes of a floating Vertical Axis Wind Turbine, Journal of Physics: Conference Series, https://doi.org/10.1088/1742-6596/1618/6/062053, 2020.

Bertelè, M., Bottasso, C., Cacciola, S., Daher Adegas, F., and Delport, S.: Wind inflow observation from load harmonics, Wind Energy Science, 2, 615–640, https://doi.org/10.5194/wes-2-615-2017, publisher: Copernicus GmbH, 2017.

Bossanyi, E.: Individual blade pitch control for load reduction, Wind Energy, https://doi.org/10.1002/we.76, 2003.

Bossanyi, E., Fleming, P., and Wright, A.: Validation of individual pitch control by field tests on two-and three-bladed wind turbines, IEEE Transactions on Control Systems Technology, https://doi.org/10.1109/TCST.2013.2258345, 2013.

Bottasso, C., Cacciola, S., and Schreiber, J.: Local wind speed estimation, with application to wake impingement detection, Renewable Energy, https://doi.org/10.1016/j.renene.2017.09.044, 2018.

Brandetti, L., Liu, Y., Pamososuryo, A., Mulders, S., Watson, S., and van Wingerden, J.W.: Unscented Kalman filter-based blade-effective wind speed estimation for a vertical-axis wind turbine, IFAC-PapersOnLine, 56, 8393–8399, https://doi.org/10.1016/j.ifacol.2023.10.1033, 2023.

Caprace, D.-G., Chatelain, P., and Winckelmans, G.: Lifting line with various mollifications: theory and application to an elliptical wing, AIAA Journal, https://doi.org/10.2514/1.J057487, 2019.

Chatelain, P., Backaert, S., Winckelmans, G., and Kern, S.: Large Eddy Simulation of Wind Turbine Wakes, Flow, Turbulence and Combustion, https://doi.org/10.1007/s10494-013-9474-8, 2013.

Chatelain, P., Duponcheel, M., Caprace, D.-G., Marichal, Y., and Winckelmans, G.: Vortex particle-mesh simulations of vertical axis wind turbine flows: from the airfoil performance to the very far wake, Wind Energy Science, https://doi.org/10.5194/wes-2-317-2017, 2017.

Chui, C., Chen, G., et al.: Kalman filtering, Springer, 2017.

Coquelet, M., Bricteux, L., Lejeune, M., and Chatelain, P.: Biomimetic individual pitch control for load alleviation, Journal of Physics: Conference Series, https://doi.org/10.1088/1742-6596/1618/2/022052, 2020.

Coquelet, M., Bricteux, L., Moens, M., and Chatelain, P.: A reinforcement-learning approach for individual pitch control, Wind Energy, https://doi.org/10.1002/we.2734, 2022.

Docquier, N., Poncelet, A., and Fisette, P.: ROBOTRAN: A powerful symbolic gnerator of multibody models, Mechanical Sciences, https://doi.org/10.5194/ms-4-199-2013, 2013.

Drécourt, J.-P., Madsen, H., and Rosbjerg, D.: Bias aware Kalman filters: Comparison and improvements, Advances in Water Resources, 29, 707–718, https://doi.org/10.1016/j.advwatres.2005.07.006, 2006.

Fleming, P., Gebraad, P., Lee, S., van Wingerden, J.W., Johnson, K., Churchfield, M., Michalakes, J., Spalart, P., and Moriarty, P.: Evaluating techniques for redirecting turbine wakes using SOWFA, Renewable Energy, https://doi.org/10.1016/j.renene.2014.02.015, 2014.

Frederik, J. and van Wingerden, J.W.: On the load impact of dynamic wind farm wake mixing strategies, Renewable Energy, https://doi.org/10.1016/j.renene.2022.05.110, 2022.

Frederik, J., Doekemeijer, B., Mulders, S., and van Wingerden, J.W.: The helix approach: Using dynamic individual pitch control to enhance wake mixing in wind farms, Wind Energy, https://doi.org/10.1002/we.2513, 2020.

Friedland, B.: Treatment of bias in recursive filtering, IEEE Transactions on Automatic Control, 14, 359–367, https://doi.org/10.1109/TAC.1969.1099223, 1969.

Hansen, M.: Aerodynamics of wind turbines, Routledge, 2015.

https://doi.org/10.5194/wes-2024-56
Preprint. Discussion started: 15 May 2024

Jonkman, J., Butterfield, S., Musial, W., and Scott, G.: Definition of a 5-MW reference wind turbine for offshore system development, National Renewable Energy Lab, 2009.

Korb, H., Asmuth, H., and Ivanell, S.: The characteristics of helically deflected wind turbine wakes, Journal of Fluid Mechanics, 965, A2, https://doi.org/10.1017/jfm.2023.390, 2023.

Lejeune, M., Moens, M., and Chatelain, P.: A meandering-capturing wake model coupled to rotor-based flow-sensing for operational wind farm flow prediction, Frontiers in Energy Research, https://doi.org/10.3389/fenrg.2022.884068, 2022.

Letizia, S., Brugger, P., Bodini, N., Krishnamurthy, R., Scholbrock, A., Simley, E., Porté-Agel, F., Hamilton, N., Doubrawa, P., and Moriarty, P.: Characterization of wind turbine flow through nacelle-mounted lidars: a review, Frontiers in Mechanical Engineering, 9, https://doi.org/10.3389/fmech.2023.1261017, 2023.

Liu, Y., Pamososuryo, A., Ferrari, R., Hovgaard, T., and van Wingerden, J.W.: Blade effective wind speed estimation: A subspace predictive repetitive estimator approach, in: 2021 European Control Conference (ECC), pp. 1205–1210, IEEE, https://doi.org/10.23919/ECC54610.2021.9654981, 2021.

Liu, Y., Pamososuryo, A., Mulders, S., Ferrari, R., and van Wingerden, J.W.: The proportional integral notch and Coleman blade effective wind speed estimators and their similarities, IEEE Control Systems Letters, 6, 2198–2203, https://doi.org/10.1109/LCSYS.2021.3140171, 2022.

Lu, Q., Bowyer, R., and Jones, B.: Analysis and design of Coleman transform-based individual pitch controllers for wind-turbine load reduction, Wind Energy, 2015.

Mann, J.: Wind field simulation, Probabilistic Engineering Mechanics, https://doi.org/10.1016/S0266-8920(97)00036-2, 1998.

Meyers, J., Bottasso, C., Dykes, K., Fleming, P., Gebraad, P., Giebel, G., Göçmen, T., and van Wingerden, J.W.: Wind farm flow control: prospects and challenges, Wind Energy Science, https://doi.org/10.5194/wes-2022-24, 2022.

Moens, M., Duponcheel, M., Winckelmans, G., and Chatelain, P.: An actuator disk method with tip-loss correction based on local effective upstream velocities, Wind Energy, https://doi.org/10.1002/we.2192, 2018.

Munters, W. and Meyers, J.: Towards practical dynamic induction control of wind farms: analysis of optimally controlled wind-farm boundary layers and sinusoidal induction control of first-row turbines, Wind Energy Science, https://doi.org/10.5194/wes-3-409-2018, 2018.

Pamososuryo, A., Liu, Y., Gybel Hovgaard, T., Ferrari, R., and van Wingerden, J.W.: Convex economic model predictive control for blade loads mitigation on wind turbines, Wind Energy, 26, 1276–1298, https://doi.org/10.1002/we.2869, 2023.

Raach, S.: Important milestone: 1000 wind turbines with lidar-assisted control, Sowento, https://www.sowento.com/wp-content/uploads/2021/11/20210527-sowento-PressRelease-Goldwind.pdf, 2021.

Russell, A., Collu, M., McDonald, A., Thies, P., Keane, A., and Quayle, A.: LIDAR-assisted feedforward individual pitch control of a 15 MW floating offshore wind turbine, Wind Energy, n/a, https://doi.org/10.1002/we.2891, 2024.

Scholbrock, A., Fleming, P., Schlipf, D., Wright, A., Johnson, K., and Wang, N.: Lidar-enhanced wind turbine control: Past, present, and future, in: 2016 American Control Conference (ACC), pp. 1399–1406, IEEE, https://doi.org/10.1109/ACC.2016.7525113, 2016.

Selvam, K., Kanev, S., van Wingerden, J.W., van Engelen, T., and Verhaegen, M.: Feedback–feedforward individual pitch control for wind turbine load reduction, International Journal of Robust and Nonlinear Control, https://doi.org/10.1002/rnc.1324, 2009.

Simley, E. and Pao, L.: Evaluation of a wind speed estimator for effective hub-height and shear components, Wind Energy, 19, 167–184, https://doi.org/10.1002/we.1817, 2016.

Snel, H. and Schepers, J.: Joint investigation of dynamic inflow effects and implementation of an engineering method, in: 1993 ECWEC Conference, ECWEC, 1995.

https://doi.org/10.5194/wes-2024-56
Preprint. Discussion started: 15 May 2024

United Nations: Transforming our world: the 2030 Agenda for Sustainable Development, https://wedocs.unep.org/20.500.11822/9814, 2015.

van Vondelen, A., Ottenheym, J., Pamososuryo, A., Navalkar, S. T., and van Wingerden, J.W.: Phase Synchronization for Helix Enhanced Wake Mixing in Downstream Wind Turbines, IFAC-PapersOnLine, 56, 8426–8431, https://doi.org/10.1016/j.ifacol.2023.10.1039, 2023a.

van Vondelen, A. A. W., Navalkar, S. T., Kerssemakers, D. R., and Van Wingerden, J.W.: Enhanced wake mixing in wind farms using the Helix approach: A loads sensitivity study, in: 2023 American Control Conference (ACC), pp. 831–836, https://doi.org/10.23919/ACC55779.2023.10155965, 2023b.

Wagenaar, J., Machielse, L., and Schepers, J.: Controlling wind in ECN's scaled wind farm, Proc. Europe Premier Wind Energy Event, 2012.

Yilmaz, A. and Meyers, J.: Optimal dynamic induction control of a pair of inline wind turbines, Physics of Fluids, https://doi.org/10.1063/1.5038600, 2018.